IEEE Access
Multidisciplinary ⋮ Rapid Review ⋮ Open Access Journal

Received 29 September 2023, accepted 12 October 2023, date of publication 17 October 2023, date of current version 23 October 2023.

Digital Object Identifier 10.1109/ACCESS.2023.3325352

RESEARCH ARTICLE

HyLoc: An Indoor Single-Site Hybrid Localization Scheme Based on LOS/NLOS Identification

JINBO ZHANG[1], HAO SUN[2], YUJIE FENG[2], AND JIANCUN FAN[2], (Senior Member, IEEE)
[1]Science and Technology on Communication Networks Laboratory, The 54th Research Institute of CETC, Shijiazhuang 050081, China
[2]School of Electronic and Information Engineering, Xi'an Jiaotong University, Xi'an, Shaanxi 710049, China

Corresponding author: Jiancun Fan (fanjc0114@gmail.com)

This work was supported by the Research Foundation of Science and Technology on Communication Networks Laboratory under Grant HHX21641X010.

ABSTRACT The complex indoor structure not only introduces *line-of-sight* (LOS) paths but also *non-line-of-sight* (NLOS) paths, which poses a huge challenge to localization. However, most of the existing indoor localization schemes only utilize a single positioning algorithm for LOS or NLOS environments, resulting in poor positioning robustness. To solve this problem, we propose an indoor single-site hybrid localization scheme called HyLoc in this paper. HyLoc combines multiple positioning algorithms and gives full play to the advantage of each algorithm in either LOS or NLOS environment. In this scheme, a *threshold judger* (TJ) is firstly designed to identify whether there is a LOS path depending on the time-domain statistical features extracted from *channel state information* (CSI). According to the identification results of TJ, HyLoc adaptively selects the optimal positioning algorithm. In the LOS environment, an improved *multiple signal classification algorithm* (MUSIC) based on forward smoothing technology is applied to obtain the estimated positioning results. In the NLOS environment, a multipath subspace projection and *extreme learning machine* (ELM)-based fingerprint localization algorithm is proposed for positioning analysis. Finally the experimental results verify that the proposed HyLoc can realize single-site localization and it has higher positioning accuracy than traditional ones in the mixed LOS and NLOS environment.

INDEX TERMS Indoor single-site hybrid localization, LOS/NLOS identification, multipath signal subspace, extreme learning machine.

I. INTRODUCTION

With the extensive applications of the wireless networks, *location-based service* (LBS) is becoming a crucial task in the era of *Internet of Things* (IOT) [1], [2] [3]. The *global navigation satellite system* (GNSS) performs well in outdoor scenarios. While in complex indoor environments, due to the fading of satellite signals and the influence of multipaths, the GNSS system has large position error and is not suitable for indoor positioning [4], [5]. Therefore, many indoor positioning schemes based on Wi-Fi, Bluetooth, ZigBee, etc. have been proposed to guarantee the indoor positioning accuracy [6].

The existing indoor positioning methods can be roughly divided into two categories: range-based and range-free. Range-based methods usually depend on the estimation of *time of arrival* (TOA), *direction of arrival* (DOA), *angle of arrival* (AOA), etc [7], [8]. These estimated ranging parameters will be used to calculate the coordinate of the target [9]. Therefore, the positioning accuracy is directly affected by the estimated error of these ranging parameters [10]. In order to improve the accuracy of these estimated parameters in the complex indoor environment, many super-resolution estimation algorithms are proposed to distinguish *line-of-sight* (LOS) signal and *non-line-of-sight* (NLOS) signals in space or time domain. Among them, the *multiple signal classification algorithm* (MUSIC) [11] and the *estimation of signal parameters via rotational invariance technique* (ESPRIT) [12] are the two most classic algorithms. Different from the range-based methods which are based on ranging measurements for localization, the range-free methods make no assumptions about the accessibility of such information. In the recent years, as the most promising and popular method among existing range-free methods, fingerprint-based positioning method has drawn wide attention in both academia and industry [13]. The key

The associate editor coordinating the review of this manuscript and approving it for publication was Aysegul Ucar.

for the fingerprint-based positioning method is to establish the mapping relationship between the actual locations and the signal characteristic fingerprints [14]. *Received signal strength* (RSS) [15] and *channel state information* (CSI) [16] are generally used as raw data to extract signal features and establish the fingerprint database. Considering that CSI describes both amplitude and phase which contain the fine-grained information of the channel path loss, shadowing, orientation and delay during the signal transmission, the performance of using CSI for positioning is much better than that of using RSS [17]. Radar and Horus are the two representative RSS-based positioning methods [18], [19]. A *fine-grained indoor fingerprint system* (FIFS) exploring the frequency-domain CSI over all subcarriers has been proposed in [20]. A large number of machine-learning algorithms, including *convolutional netural network* (CNN), *random forest* (RF), and *support vector machine* (SVM) [21], [22], [23], are widely used to establish the mapping relationship between location coordinates and fingerprints.

In general, the method depending on the estimation of ranging parameters and the fingerprint-based positioning method are the two most commonly used indoor positioning methods. These methods actually have their own pros and cons. The positioning accuracy of range-based methods is usually higher than that of fingerprint-based. However, in order to guarantee the estimated accuracy of the ranging parameters, it is necessary to ensure the existence of LOS path in the indoor environment. While in the NLOS case, the signals are reflected and scattered due to the obstacles, resulting in large error bias of the positioning parameter estimation [24]. The large parameter estimation error will lead to poor positioning performance. Therefore, the range-based methods is more suitable for LOS conditions. For the fingerprint-based method, the geometric relationship between the terminal and the target does not need to be considered. This method is less affected by the environment and has higher robustness and reliability, so it has higher accuracy in NLOS condition.

However, when it comes to indoor localization, it becomes a huge challenge since the indoor scenarios are actually mixed LOS and NLOS environments [25], [26]. Most existing indoor localization schemes only utilize a single positioning algorithm, resulting in poor positioning robustness. In order to achieve high positioning accuracy in both NLOS and LOS scenarios, combining multiple methods is an effective solution. Generally, the solutions to indoor localization problems under mixed LOS and NLOS conditions can be classified into three categories: 1) mathematical optimizations [27], [28], [29], 2) robust estimation techniques [30], [31], 3) LOS/NLOS identification [32], [33]. The indoor localization approaches relying on LOS/NLOS identification are the main focus of this paper. The machine-learning-based techniques are usually used for LOS/NLOS identification [34]. However, these techniques rely on additional experimental campaigns to build up a database, which is very time-consuming and hard to apply in practice. Reference [35] proposed a millimeter-wave LOS/NLOS identification scheme utilizing mean-shift clustering algorithm and a 3D AOA localization algorithm for both LOS and one-bound reflection NLOS paths. Though the estimation bias are corrected using LOS/NLOS identification, the single AOA localization algorithm limits the position accuracy to some extent. In [36], a dynamic positioning method based on RSS is proposed to improve the accuracy and stability of positioning results. The mixed Gauss model is firstly adopted to describe the LOS and NLOS propagation effects and at the same time, the *simulated annealing* (SA) algorithm is exploited to overcome the local optimal solution problem. While, as the coarse-grained parameter, the position performance of RSS-based methods is actually worse than that of CSI-based methods. In [37], 8 features were extracted from the received signal to identify the LOS and NLOS conditions. And in the NLOS environment, the ranging results were adjusted to mitigate the influence of NLOS.

The research of positioning schemes in mixed LOS/NLOS indoor environments is very challenging. What's more, though LOS/NLOS identification is applied to correct the estimation error bias under NLOS environments, the error bias cannot be corrected completely and the improvement of positioning accuracy is limited by only using a single positioning algorithm. To deal with these problems, we propose a new indoor single-site hybrid localization scheme based on LOS/NLOS identification called HyLoc. In a single station positioning scenario, instead of using machine-learning-based methods which are hard to apply in practice, a *threshold judger* (TJ) is firstly designed to identify whether there is a LOS path depending on the time-domain statistical features extracted from CSI. According to the results of LOS/NLOS identification, HyLoc adaptively selects the optimal positioning algorithm. In the LOS environment, an improved multiple signal classification algorithm (MUSIC) based on forward smoothing technology is applied to get the estimated TOA and DOA. The *least squares* (LS) method is then applied to calculate the coordinate of the target based on these parameters. In the NLOS environment, a *multipath subspace projection* (MSP) and *extreme learning machine* (ELM)-based indoor fingerprint localization algorithm is proposed in this paper to realize localization. In this algorithm, the CSI is firstly organized into a time-domain matrix and then is projected into a subspace. This processing not only preserves the channel multipath information as much as possible, but also reduces the data dimension. Based on the reduced dimension projected data, an ensemble of ELM networks is exploited to implement the fingerprint localization. HyLoc combines multiple positioning algorithms and gives full play to the advantage of each algorithm in either LOS or NLOS environment. Finally, the experiment verifies that the proposed HyLoc can realize single-site localization and has better positioning effect than the single method and other existing position-

ing schemes. In summary, our main contributions are as follows.

1) We propose an indoor single-site hybrid localization scheme based on LOS/NLOS identification called HyLoc in this paper.
2) We design an easy-to-apply TJ to distinguish whether there is a LOS path effectively in HyLoc.
3) We propose the MSP and ELM-based method to complete fingerprint localization in HyLoc.

Following the introduction, we will describe the measurement model in Section II. Section III presents the proposed HyLoc in details. The positioning results are analyzed under the experimental data in Section IV. Finally, the conclusion is drawn in Section V.

II. MEASUREMENT MODEL

As mentioned above, CSI and RSS are commonly measured as raw data for positioning analysis. In the view of the fact that CSI has the advantages of stable state and rich information, it is used for localization in this paper. CSI describes the channel characteristics of the communication link at the physical layer. It not only provides channel information such as environmental attenuation and distance attenuation, but also shows the reflection, scattering and diffraction of signal transmission in the indoor environment. In this paper, the *orthogonal frequency division multiplexing* (OFDM) system is used when we collect the data. Assuming there is a target to be located and a base station with a known location, the target sends OFDM signal to the base station for positioning. The signal model is formulated as

$$\boldsymbol{Y} = \boldsymbol{H}\boldsymbol{X} + \boldsymbol{Z}, \tag{1}$$

where $\boldsymbol{Y}$ is the received signal vector, $\mathbf{X}$ is the transmitted signal vector, $\boldsymbol{H}$ is the CSI matrix and $\boldsymbol{Z}$ represents the additional Gaussian white noise vector. The receiver estimates the CSI matrix $\boldsymbol{H}$ using the pre-defined signal $\boldsymbol{X}$ and the receive signal $\boldsymbol{Y}$. The CSI matrix can be estimated by the following formula

$$\hat{\boldsymbol{H}} = \frac{\boldsymbol{Y}}{\boldsymbol{X}}, \tag{2}$$

where $\hat{\boldsymbol{H}}$ is the estimated CSI.

In the OFDM system, the signal is transmitted through multiple subcarriers. CSI represents the channel gain vector of each subcarrier. It describes the process where wireless signals propagate from the transmitter to the receiver at a specific carrier frequency. The CSI can be expressed as

$$\boldsymbol{H} = [H_1, H_2, \cdots, H_K], \tag{3}$$

where K is the number of the subcarriers. H_k denotes the CSI of the k-th subcarrier and can be expressed as

$$H_k = |H_k| \, e^{j\phi_k}, \tag{4}$$

where $|H_k|$ and ϕ_k respectively denote the CSI amplitude and phase of the k-th subcarrier.

When the device is connected to the wireless network, the data of each subchannel is extracted through modulation and demodulation, and the CSI data packet can be obtained. During the transmission process, due to the interference of ambient noise and hardware limitations, the phase will shift. Therefore it is necessary to preprocess the CSI data to obtain more stable phase information. *Carrier frequency offset* (CFO) and *sampling frequency offset* (SFO) are mainly considered in this paper. The phase measured on the k-th subcarrier $\widehat{\phi_k}$ can be expressed as [38].

$$\widehat{\phi_k} = \phi_k + 2\pi \frac{k}{N} \Delta t + \rho + Z, \tag{5}$$

where ϕ_k is the true phase of the k-th subcarrier, Δt denotes the sampling interval, N is the size of the fast Fourier transform, Z denotes the noise and ρ denotes the phase shift caused by carrier frequency error.

It can be seen that the sampling frequency offset $2\pi \frac{k}{N} \Delta t$ is a linear function related to the subcarrier index k. We can perform a linear transformation on the original phase to remove the influence of Δt and β. Let λ_{PS} and λ_{PO} respectively denote the phase slope and the phase offset over the entire frequency band, then λ_{PS} and λ_{PO} can be estimated as follows [38].

$$\begin{aligned} \lambda_{PS} &= \frac{\widehat{\phi_k} - \widehat{\phi_1}}{k - 1} \\ \lambda_{PO} &= \frac{1}{K} \sum_{k=1}^{K} \widehat{\phi_k}, \end{aligned} \tag{6}$$

where $\widehat{\phi_k}$ and $\widehat{\phi_1}$ respectively denote the phase measurement of the k-th subcarrier and the first subcarrier.

The corrected phase $\tilde{\phi_k}$ of the k-th subcarrier can be finally obtained by subtracting $k\lambda_{PS} + \lambda_{PO}$ from the original measured phase

$$\tilde{\phi_k} = \widehat{\phi_k} - k\lambda_{PS} - \lambda_{PO}. \tag{7}$$

In the main body of the paper, we will use the phase-corrected CSI for positioning analysis.

III. THE HYBRID POSITIONING SCHEME BASED ON LOS/NLOS IDENTIFICATION

In this section, we will propose a hybrid positioning scheme based on LOS/NLOS identification, whose block diagram is shown in Fig. 1 and its flowchart illustrating the steps is depicted in Fig. 2. The HyLoc system consists of two main parts: an off-line training phase and an on-line positioning phase. In the off-line training phase, we construct an off-line map and preprocess the data to generate the ELM network for all training points that involve NLOS paths. In the on-line positioning phase, we will execute the LOS/NLOS identification based on the TJ and the hybrid positioning scheme based on the LOS/NLOS identification result. Firstly, the TJ based on the statistical features of CSI is designed to determine whether the environment is LOS or NLOS. In the second stage, specific methods are applied separately,

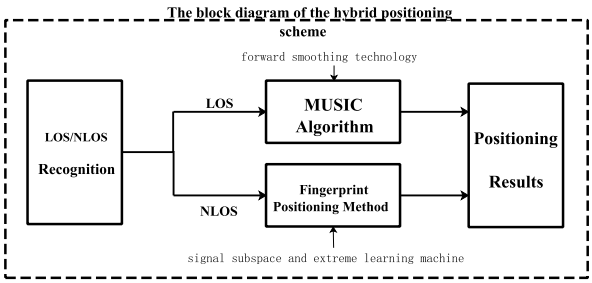

FIGURE 1. The overall framework of the HyLoc.

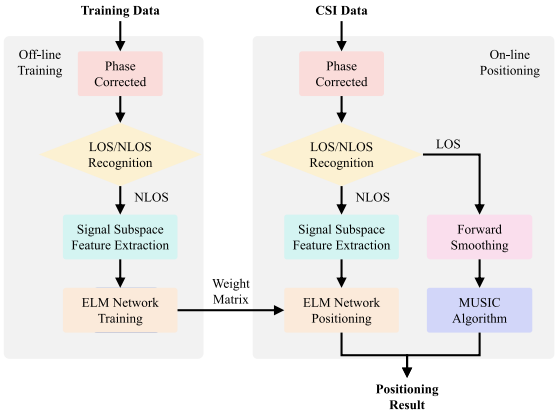

FIGURE 2. The flowchart of the HyLoc.

depending on the identified LOS or NLOS environment, to obtain precise positioning results. For the anchor points with LOS path, an improved MUSIC algorithm based on forward smoothing technology is used to estimate the ranging parameters. Then the LS method is applied to calculate the coordinate of the target based on these parameters. For the anchor points with NLOS paths, the fingerprint positioning method based on MSP and ELM is adopted. According to the corresponding sight conditions at different anchor points, the HyLoc combines multiple positioning algorithms to improve positioning performance.

A. THRESHOLD JUDGER BASED ON CSI STATISTICAL FEATURES FOR LOS/NLOS RECOGNITION

An easy-to-apply TJ is designed to complete the LOS/NLOS recognition. After extracting the CSI, four statistical features are firstly calculated based on the time domain signal measurements. According to the differences of these statistical features in different environments, the threshold comparison method is then used to classify each feature. The thresholds can be determined by the data observation of the sampling points. A weighted logic detector is finally used to complete the final recognition. The specific mathematical model of the LOS/NLOS recognition algorithm is described as follows.

Suppose there is a classification problem

$$\vartheta = \begin{cases} 1 & \text{LOS} \\ 0 & \text{NLOS}. \end{cases} \tag{8}$$

We distinguish between LOS and NLOS environments based on different probability distributions of *received signal power* (RSP). The channel measurement values are continuously observed at the receiver. For the CSI data, we hold that its amplitude value reflects the power of the received signal. Therefore, we select the amplitude value of the CSI at the first subcarrier as the measurement value of the RSP.

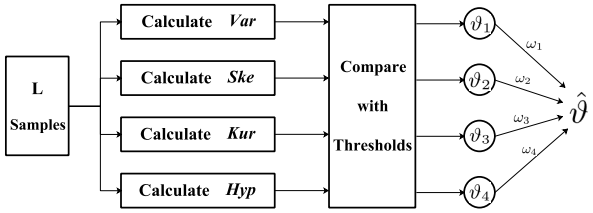

FIGURE 3. Threshold judger.

Define the amplitude value of the CSI at the first subcarrier as h^0, and the observed RSP vector can be expressed as $\boldsymbol{h}^0 = [h_1^0, h_2^0, \ldots, h_L^0]$, where L denotes the channel measurement length.

We assume that the RSP measurement value is a random variable $\boldsymbol{h}$. The probability density function of the random variable $\boldsymbol{h}$ can be used to describe whether the channel has a LOS path. For a given RSP measurement vector, define the p-th moment of the random variable $\boldsymbol{h}$ as

$$m_p = \frac{1}{L}\sum_{i=1}^{L}\left(h_i^0 - \mu\right)^p, \tag{9}$$

$$\mu = \frac{1}{L}\sum_{i=1}^{L} h_i^0. \tag{10}$$

Through a large number of the RSP measurement samples, the following four statistical characteristics can be got

- the variance $Var = \sqrt{m_2}$,
- the skewness $Ske = m_3/Var^3$,
- the kurtosis $Kur = m_4/Var^4$,
- the hyperskewness $Hyp = m_5/Var^5$,

where Skewness, kurtosis, and overskewness are called third-order, fourth-order, and fifth-order normalized moments, respectively.

It can be known that in the LOS environment, the probability distribution of RSP is similar to the Weibull distribution, while in the NLOS environment, the probability distribution of RSP approximates the Gaussian distribution. Based on the difference of the RSP probability distribution in LOS and NLOS environments, a TJ is designed in this paper to distinguish different channel environments, and the structure of the TJ is shown in Fig. 3.

In the TJ, the four statistical features $\{Var, Ske, Kur, Hyp\}$ are firstly compared with the thresholds $\{Var^*, Ske^*, Kur^*, Hyp^*\}$ respectively to get four new indicators $\{\vartheta_1, \vartheta_2, \vartheta_3, \vartheta_4\}$. The final channel state is then obtained by the weighted summation of these four new indicators. These four indicators are calculated as follows.

$$\vartheta_1 = \begin{cases} 1 & \text{if } Var \le Var^* \\ 0 & \text{otherwise} \end{cases}, \vartheta_2 = \begin{cases} 1 & \text{if } Ske \le Ske^* \\ 0 & \text{otherwise} \end{cases}, \tag{11}$$

$$\vartheta_3 = \begin{cases} 1 & \text{if } Kur \le Kur^* \\ 0 & \text{otherwise} \end{cases}, \vartheta_4 = \begin{cases} 1 & \text{if } Hyp \le Hyp^* \\ 0 & \text{otherwise} \end{cases} \tag{12}$$

According to the basic principle of the statistical model, this LOS/NLOS identification algorithm is reasonable and feasible. The statistical distribution of RSP in the LOS environment is steeper because the RSP tends to be concentrated around the direct path component. While in the NLOS environment, multiple reflection paths have great impact on the received signal, resulting in a flatter distribution. Therefore, the value of *Var* is smaller and the value of *Kur* is larger in LOS environment. These four statistical characteristics can be used to determine whether there is a LOS path. Considering that these four features may have different confidence levels, different values can be taken for the weighting coefficients. The weighting coefficients $\boldsymbol{\omega} = [\omega_1, \omega_2, \omega_3, \omega_4]$ must meet the following conditions

$$\sum_{i=1}^{4} \omega_i = 1, \text{ and } \omega_i \in [0, 1]. \tag{13}$$

The final decision index $\hat{\vartheta}$ is obtained by the weighted summation of these four indicators

$$\hat{\vartheta} = \sum_{i=1}^{4} \omega_i \vartheta_i. \tag{14}$$

Finally, the channel state identification can be expressed as

$$\vartheta = \begin{cases} 1 & \text{if} \hat{\vartheta} \ge 0.5 \\ 0 & \text{otherwise,} \end{cases} \tag{15}$$

where $\vartheta = 1$ denotes the LOS environment and $\vartheta = 0$ denotes the NLOS environment.

It can be noted that when $\omega_i = 1/4$, this method is equivalent to an unweighted multi-threshold detector. The weights can be modulated according to the actual environment, so that the features with greater difference in different channel states will have larger weights in order to get higher precision recognition results.

The thresholds $\{Var^*, Ske^*, Kur^*, Hyp^*\}$ and the weighting coefficients $\{\omega_1, \omega_2, \omega_3, \omega_4\}$ of the weighted logic detector can be obtained from a large number of the RSP measurement samples. These measurement samples can basically describe the probability distribution of each statistical feature. The thresholds and weights are determined based on the following criteria: the probability of the misjudgment of the statistical feature should be minimized by the selection of the threshold values, and the weighting coefficients are selected according to the probability of the misjudgment of the channel identification result after the feature thresholds are determined.

B. AN IMPROVED MUSIC ALGORITHM BASED ON FORWARD SMOOTHING TECHNOLOGY

In the LOS environment, an improved MUSIC algorithm based on forward smoothing technology is used to estimate the ranging parameters. And then the LS method is applied to calculate the coordinate of the target based on these parameters.

The principle of the MUSIC algorithm is based on the phase difference between different antennas when the signals arrive at the antenna array. In the multipath environment, the array response of the r-th antenna can be expressed as

$$\Psi_{r,\theta_p} = e^{-j2\pi f_k (r-1) d \sin\theta_p / c}, \tag{16}$$

where θ_p is the direction of arrival of the p-th path, d denotes the spacing between adjacent antennas, f_k denotes the subcarrier frequency of the k-th subcarrier and c denotes the speed of light.

In addition to the phase difference caused by the antenna spacing, the phase difference is also caused due to the different frequency of each subcarrier. The frequency response of the k-th subcarrier can be expressed as

$$\Omega_{k,\tau_p} = e^{-j2\pi f_k \tau_p}, \tag{17}$$

where τ_p denotes the propagation time of the p-th path.

It can be known that the MUSIC algorithm is effective only under the condition that the number of receiving antennas is more than the number of multipaths. Based on the technology of OFDM, the method of expanding the virtual antennas is used to break through this limitation in this paper. Assuming the CSI matrix collected in practice contains k subcarriers and r receiver antennas, the received CSI matrix $\boldsymbol{H}$ can be expressed as

$$\boldsymbol{H} = \begin{bmatrix} H_{1,1} & H_{1,2} & \cdots & H_{1,k} \\ H_{2,1} & H_{2,2} & \cdots & H_{2,k} \\ \vdots & \vdots & \vdots & \vdots \\ H_{r,1} & H_{r,2} & \cdots & H_{r,k} \end{bmatrix}. \tag{18}$$

Among them, $H_{r,k}$ represents the CSI value of the k-th subcarrier on the r-th antenna. We write the matrix $\boldsymbol{H}$ as a column, that is, expand r antennas into $r \times k$ virtual antennas

$$\tilde{\boldsymbol{H}} = [\ H_{1,1} \ \cdots \ H_{1,k} \ H_{2,1} \ \cdots \ H_{2,k} \ \cdots H_{r,1} \ \cdots \ H_{r,k} \ ]^T. \tag{19}$$

$\tilde{\boldsymbol{H}}$ is regarded as the expanded virtual array received signal and can be written as the following matrix form

$$\tilde{\boldsymbol{H}} = \boldsymbol{\Theta U} + \boldsymbol{Z}, \tag{20}$$

where $\boldsymbol{\Theta}$ is the matrix composed of the above-mentioned phase difference, $\boldsymbol{U}$ is a $p \times 1$ vector representing the multipath signal attenuation coefficient and $\boldsymbol{Z}$ is Gaussian

white noise.

$$\boldsymbol{\Theta} = \begin{bmatrix} \Psi_{1,\theta_1}\Omega_{1,\tau_1} & \Psi_{1,\theta_2}\Omega_{1,\tau_2} & \cdots & \Psi_{1,\theta_p}\Omega_{1,\tau_p} \\ \vdots & \vdots & & \vdots \\ \Psi_{1,\theta_1}\Omega_{k,\tau_1} & \Psi_{1,\theta_2}\Omega_{k,\tau_2} & \cdots & \Psi_{1,\theta_p}\Omega_{k,\tau_p} \\ \Psi_{2,\theta_1}\Omega_{1,\tau_1} & \Psi_{2,\theta_2}\Omega_{1,\tau_2} & \cdots & \Psi_{2,\theta_p}\Omega_{1,\tau_p} \\ \vdots & \vdots & & \vdots \\ \Psi_{2,\theta_1}\Omega_{k,\tau_1} & \Psi_{2,\theta_2}\Omega_{k,\tau_2} & \cdots & \Psi_{2,\theta_p}\Omega_{k,\tau_p} \\ \vdots & \vdots & & \vdots \\ \Psi_{r,\theta_1}\Omega_{1,\tau_1} & \Psi_{r,\theta_2}\Omega_{1,\tau_2} & \cdots & \Psi_{r,\theta_p}\Omega_{1,\tau_p} \\ \vdots & \vdots & & \vdots \\ \Psi_{r,\theta_1}\Omega_{k,\tau_1} & \Psi_{r,\theta_2}\Omega_{k,\tau_2} & \cdots & \Psi_{r,\theta_p}\Omega_{k,\tau_p} \end{bmatrix}, \tag{21}$$

where $\boldsymbol{\Theta}$ can also be expressed as

$$\boldsymbol{\Theta} = \left[\boldsymbol{a}\left(\theta_1, \tau_1\right) \boldsymbol{a}\left(\theta_2, \tau_2\right) \cdots \boldsymbol{a}\left(\theta_p, \tau_p\right) \right]. \tag{22}$$

After the expanded virtual array CSI $\tilde{\boldsymbol{H}}$ is obtained, the covariance matrix $\boldsymbol{R}_{\tilde{H}\tilde{H}} = E\left\{\tilde{\boldsymbol{H}}\tilde{\boldsymbol{H}}^{\mathrm{H}}\right\}$ can be calculated, and the spatial spectrum function $P_{\mathrm{MUSIC}}(\theta, \tau)$ can be constructed according to the MUSIC algorithm

$$P_{MUSIC}(\theta, \tau) = \frac{1}{\boldsymbol{a}^H(\theta, \tau)\boldsymbol{E}_n\boldsymbol{E}_n^H\boldsymbol{a}(\theta, \tau)}, \tag{23}$$

where $\boldsymbol{E_n}$ is the eigenspace matrix of $\boldsymbol{R}_{\tilde{H}\tilde{H}}$. According to the principle of the MUSIC algorithm, $\boldsymbol{E_n}$ and $\boldsymbol{a}(\theta, \tau)$ are orthogonal, so that the denominator of the space spectrum is zero. The peak of the spatial spectrum can be found by changing the angle of arrival and the time of arrival, and then the position of the receiver can be calculated depending on the coordinate of the transmitter and the estimated positioning parameters.

Under the premise that the sources are independent of each other, the angle of arrival and time of arrival of multiple sources can be estimated well using the MUSIC algorithm. Considering that there is only one transmitter, the signals reach the receiver after multiple reflections and refractions in space. Under this condition, it is obvious that the signals of each path are not completely independent. Coherent signals will seriously affect the estimation accuracy of the MUSIC algorithm. Therefore, it is necessary to remove relevant signals to improve the MUSIC algorithm performance.

Forward smoothing technology is used to solve this problem in this paper. It makes the related signals into different subarrays. As shown in the Fig. 4, the constructed $r \times k$ virtual antennas are used for smoothing. In order to smooth coherent sources into independent sources, it must be guaranteed that the number of subarray elements is larger than the number of coherent sources, and the number of subarrays is larger than or equal to the number of coherent sources [39]. We take the number of subarray elements as $\frac{k}{2}+1$ (assuming k is even) and the number of subarrays as $r \times \frac{k}{2}$. In this way, $\tilde{\boldsymbol{H}}$ can be smoothed into a $\left(r \times \frac{k}{2}\right) \times \left(\frac{k}{2}+1\right)$ matrix

$$\tilde{\boldsymbol{H}} = \begin{bmatrix} H_{1,1} & H_{1,2} & \cdots & H_{1,\frac{k}{2}+1} \\ \vdots & \vdots & & \vdots \\ H_{1,\frac{k}{2}} & H_{1,\frac{k}{2}+1} & \cdots & H_{1,k} \\ H_{2,1} & H_{2,2} & \cdots & H_{2,\frac{k}{2}+1} \\ \vdots & \vdots & & \vdots \\ H_{2,\frac{k}{2}} & H_{2,\frac{k}{2}+1} & \cdots & H_{2,k} \\ \vdots & \vdots & & \vdots \\ H_{r,1} & H_{r,2} & \cdots & H_{r,\frac{k}{2}+1} \\ \vdots & \vdots & & \vdots \\ H_{r,\frac{k}{2}} & H_{r,\frac{k}{2}+1} & \cdots & H_{r,k} \end{bmatrix}. \tag{24}$$

$\boldsymbol{\Theta}$ is a $(r \times \frac{k}{2}) \times p$ matrix

$$\boldsymbol{\Theta} = \begin{bmatrix} \Psi_{1,\theta_1}\Omega_{1,\tau_1} & \Psi_{1,\theta_2}\Omega_{1,\tau_2} & \cdots & \Psi_{1,\theta_p}\Omega_{1,\tau_p} \\ \vdots & \vdots & & \vdots \\ \Psi_{1,\theta_1}\Omega_{\frac{k}{2},\tau_1} & \Psi_{1,\theta_2}\Omega_{\frac{k}{2},\tau_2} & \cdots & \Psi_{1,\theta_p}\Omega_{\frac{k}{2},\tau_p} \\ \Psi_{2,\theta_1}\Omega_{1,\tau_1} & \Psi_{2,\theta_2}\Omega_{1,\tau_2} & \cdots & \Psi_{2,\theta_p}\Omega_{1,\tau_p} \\ \vdots & \vdots & & \vdots \\ \Psi_{2,\theta_1}\Omega_{\frac{k}{2},\tau_1} & \Psi_{2,\theta_2}\Omega_{\frac{k}{2},\tau_2} & \cdots & \Psi_{2,\theta_p}\Omega_{\frac{k}{2},\tau_p} \\ \vdots & \vdots & & \vdots \\ \Psi_{r,\theta_1}\Omega_{1,\tau_1} & \Psi_{r,\theta_2}\Omega_{1,\tau_2} & \cdots & \Psi_{r,\theta_p}\Omega_{1,\tau_p} \\ \vdots & \vdots & & \vdots \\ \Psi_{r,\theta_1}\Omega_{\frac{k}{2},\tau_1} & \Psi_{r,\theta_2}\Omega_{\frac{k}{2},\tau_2} & \cdots & \Psi_{r,\theta_p}\Omega_{\frac{k}{2},\tau_p} \end{bmatrix}. \tag{25}$$

In this way, the new spatial spectrum can be obtained by bringing the $\boldsymbol{\Theta}$ obtained after the forward smoothing process into the original spatial spectrum expression, and the angle of arrival and the arrival time can be estimated by searching for the peak. After getting these ranging parameters, the LS method is applied to calculate the coordinate of the target.

C. FINGERPRINT POSITIONING ALGORITHM BASED ON SIGNAL SUBSPACE AND ELM IN NLOS ENVIRONMENT

In NLOS environment, a fingerprint positioning algorithm based on MSP and ELM is proposed for positioning in this paper. The algorithm can be divided into two steps: MSP feature extraction and ELM network implementation.

1) MULTIPATH SIGNAL SUBSPACE FEATURE EXTRACTION

The simulation data in this paper is collected using the *long term evolution* (LTE) system. According to the LTE system protocol, we choose 10MHz as the signal bandwidth and sent 31500 OFDM symbols, with a duration of approximately 0.2 seconds. Therefore the final extracted CSI is a $600 \times 31500 \times 2 \times 2$ tensor at each grid point, representing 600 subcarriers in the frequency domain, 31500 OFDM sysbols in the time domain and 2×2 *multi-input multi-output* (MIMO) in the spatial domain. Considering that the signal receiver we are using in the data collection stage

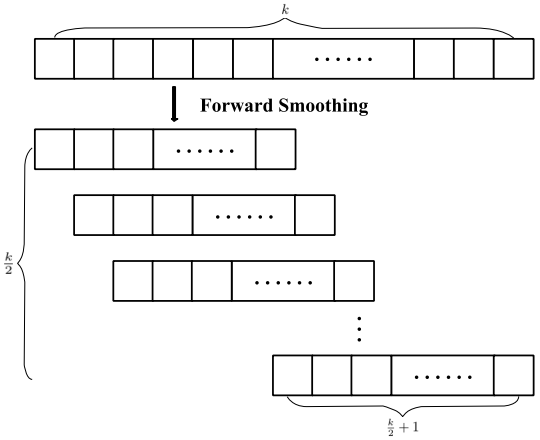

FIGURE 4. Schematic diagram of forward smoothing method.

has a receiving cycle period of 1260 OFDM symbols, and 31500 OFDM symbols contain 25 complete receiving cycles. So we split the original CSI data into 25 parts and use the split parts to construct fingerprints separately. We will finally construct 25 fingerprints at each grid point. However, the feature dimension of each fingerprint is $600 \times 1260 \times 2 \times 2 = 302400$, which is too high to be used as an input to the neural network. Thence it is necessary to do data dimensionality reduction without losing useful information.

In this paper, we use the basic idea of SP based on multipath signal propagation model to perform dimensionality reduction and feature extraction on CSI. The multipath SP algorithm in [40] is extended by using multiple snapshots. The multipath *channel frequency response* (CFR) of the k-th subcarrier and r-th antenna element at i-th OFDM symbol takes the form as

$$H_{r,k}(i) = \sum_{p=0}^{P-1} \alpha_p(i) e^{-j2\pi(f_c + k\Delta f)(\tau_p(i) + \tau_r(\theta_p))} + n_{r,k}(i), \quad (26)$$

where i denotes the index of the i-th OFDM symbol, P is the number of multipath components, $\alpha_p(i)$ denotes the distance-dependent complex attenuation of the p-th path, which is usually unknown in most cases. Δf denotes the subcarrier spacing, f_c denotes the carrier frequency, and $n_{r,k}(i)$ denotes additive white measurement noise with mean zero and variance σ^2 for the r-th antenna and the k-th subcarrier at i-th OFDM symbols.

It is reasonable to assume that the multipath delays at different symbols are similarly constant, so we can simplify $\tau_p(i)$ into τ_p. $\tau_r(\theta_p) = r\tau(\theta_p)$ denotes the propagation time difference of the impinging wave between the r-th antenna and the reference antenna. Meanwhile, due to the effect of time delay across the antenna element is much smaller than the path delay, after proper approximation, $e^{-j2\pi(f_c + k\Delta f)\tau_r(\theta_p)}$ can be also represented as $e^{-j2\pi f_c r\tau(\theta_p)}$. Considering the array element spacing is usually equal to the half-wavelength of incident signal, we have $\lambda/2 = c/2f_c$, where λ denotes the signal wavelength. Therefore, $e^{-j2\pi f_c r\tau(\theta_p)}$ can be simplified as $e^{-jr\pi \sin\theta_p}$. Eventually, the elements of CFR matrix in (26) can be rewritten as

$$H_{r,k}(i) = \sum_{p=0}^{P-1} \alpha_p(i) e^{-j2\pi f_c \tau_p} e^{-j2\pi k\Delta f \tau_p} e^{-jr\pi \sin\theta_p} + n_{r,k}(i). \quad (27)$$

Considering the correlation of the CSI at multiple adjacent subcarriers, we average the frequency responses of a certain number of subcarriers, and express the time-domain CSI sequence for the r-th antenna at different OFDM symbols as follows

$$\begin{aligned} x_r(i) &= \frac{1}{K}\sum_k H_{r,k}(i) \\ &= \frac{1}{K}\sum_k \sum_{p=0}^{P-1} \alpha_p(i) e^{-j2\pi f_c \tau_p} e^{-j2\pi k\Delta f \tau_p} e^{-jr\pi \sin\theta_p} \\ &\quad + \frac{1}{K}\sum_k n_{r,k}(i) \\ &= \sum_{p=0}^{P-1} \alpha_p(i) e^{-j2\pi f_c \tau_p} e^{-jr\pi \sin\theta_p} \sum_k \frac{1}{K} e^{-j2\pi k\Delta f \tau_p} \\ &\quad + \sum_k \frac{1}{K} n_{r,k}(i). \end{aligned} \quad (28)$$

Considering there are I symbols in a snapshot, we can rewrite (28) using vector notation as follows

$$\boldsymbol{x}_r = \boldsymbol{A}_r \boldsymbol{\gamma} + \boldsymbol{n}_r, \quad (29)$$

where $\boldsymbol{x}_r$ and $\boldsymbol{n}_r$ are the $I \times 1$ vectors, I is the number of symbols in a receiving cycle period,

$$\begin{aligned} \boldsymbol{x}_r &= [x_r(1), x_r(2), \ldots, x_r(I)]^T \\ \boldsymbol{n}_r &= [n_r(1), n_r(2), \ldots, n_r(I)]^T. \end{aligned} \quad (30)$$

$\boldsymbol{\gamma}$ is the $P \times 1$ vector

$$\boldsymbol{\gamma} = \left[\sum_k \frac{1}{K} e^{-j2\pi k\Delta f \tau_0}, \quad \ldots \quad , \sum_k \frac{1}{K} e^{-j2\pi k\Delta f \tau_{P-1}}\right]^T, \quad (31)$$

and $\boldsymbol{A}_r$ is the $I \times P$ matrix

$$\begin{aligned} \boldsymbol{A}_r = [&e^{-j2\pi f_c \tau_0} e^{-jr\pi \sin\theta_0} \boldsymbol{\alpha}_0, \\ &\ldots, e^{-j2\pi f_c \tau_{P-1}} e^{-jr\pi \sin\theta_{P-1}} \boldsymbol{\alpha}_{P-1}], \end{aligned} \quad (32)$$

with $\boldsymbol{\alpha}_p$ being the $I \times 1$ vector

$$\boldsymbol{\alpha}_p = \left[\alpha_p(1), \alpha_p(2), \ldots, \alpha_p(I)\right]^T. \quad (33)$$

Since the noise can be decoupled from the uniqueness problem by its nature, we ignore the noise. Suppose we divide all the subcarriers into U parts, we average the frequency responses of a certain number of subcarriers separately. The U sets of the vector $\boldsymbol{x}_r$ can be expressed as

$$\boldsymbol{X} = \boldsymbol{A}(\Theta, \mathrm{T})\Gamma, \quad (34)$$

where $\boldsymbol{X}$ is the $I \times U$ matrix

$$\boldsymbol{X} = \left[\boldsymbol{x}_r^1, \ldots, \boldsymbol{x}_r^U\right]. \tag{35}$$

$\boldsymbol{\Gamma}$ is the $P \times U$ matrix

$$\boldsymbol{\Gamma} = \left[\boldsymbol{\gamma}^1, \ldots, \boldsymbol{\gamma}^U\right], \tag{36}$$

and $\boldsymbol{A}(\Theta, \mathrm{T}) \equiv \boldsymbol{A}_r$ is the $I \times P$ matrix defined in (32), with $\Theta = \{\theta_1, \ldots, \theta_{P-1}\}$ and $\mathrm{T} = \{\tau_1, \ldots, \tau_{P-1}\}$ denoting the directions of arrival and the delays of transmitter reflections.

It can be noted that the matrix $\boldsymbol{A}_r$ averages the frequency-domain channel response in the carrier domain and captures all the multipath delay and attenuation information. Therefore this matrix will be the basis of the fingerprint construction in this paper.

For the receiver, the parameters of the channel model cannot be directly known, that is, $\boldsymbol{A}_r$ cannot be obtained directly. To derive a similarity-metric for the fingerpring matching, we resort to the estimation of the matrix $\boldsymbol{A}_r$ using the Maximum Likelihood (ML) criterion [41].

Assuming $\boldsymbol{\Gamma} = \left[\gamma^1, \ldots, \gamma^U\right]$ is the frequency selective fading coefficient matrix, which are uncertain parameters that need to be estimated in conjunction with the spatial-temporal matrix $\boldsymbol{A}_r$. According to reference [41], the probability density function of the averaged CSI sequence $\boldsymbol{x}_r(i)$ can be given by

$$p\left(\boldsymbol{x}_r^1, \ldots, \boldsymbol{x}_r^U \mid \boldsymbol{A}_r, \boldsymbol{\Gamma}, \sigma^2\right) = \prod_{u=1}^{U} \frac{1}{\pi^I \det\left[\sigma^2 \boldsymbol{I}\right]} \cdot \exp\left(-\frac{1}{\sigma^2}\left\|\boldsymbol{x}_r^u - \boldsymbol{A}_r \boldsymbol{\gamma}^u\right\|^2\right). \tag{37}$$

As show in appendix A, $\boldsymbol{A}_r$ can be estimated as:

$$\begin{aligned}\widehat{\boldsymbol{A}}_r &= \arg\min_{\boldsymbol{A}_r} \sum_{u=1}^{U} \|\boldsymbol{x}_r^u - \boldsymbol{\xi}\boldsymbol{x}_r^u\|^2 \\ &= \arg\max_{\boldsymbol{A}_r} \sum_{m=1}^{M} \|\boldsymbol{\xi}\boldsymbol{x}_r^u\|^2,\end{aligned} \tag{38}$$

where $\boldsymbol{\xi}$ is the projection matrix in the column span direction of $\boldsymbol{A}_r$

$$\boldsymbol{\xi} = \boldsymbol{A}_r \left(\boldsymbol{A}_r^H \boldsymbol{A}_r\right)^{-1} \boldsymbol{A}_r^H. \tag{39}$$

It can be easily proved that equation(38) can also be written as

$$\widehat{\boldsymbol{A}}_r = \arg\max_{\boldsymbol{A}_r} \mathrm{Tr}\left\{\boldsymbol{\xi}\widehat{\boldsymbol{R}}\right\}, \tag{40}$$

where $\mathrm{Tr}\{\cdot\}$ denotes the trace of the matrix, and $\widehat{\boldsymbol{R}}$ denotes the covariance matrix of the averaged CSI sequences

$$\widehat{\boldsymbol{R}} = \frac{1}{U} \sum_{u=1}^{U} \boldsymbol{x}_r^u \boldsymbol{x}_r^{uH}. \tag{41}$$

From the above derivation, it can be seen that the estimation of $\boldsymbol{A}_r$ is related to $\boldsymbol{\xi}$ and $\widehat{\boldsymbol{R}}$. Therefore we can map $\mathbf{A}$ to the subspace $\boldsymbol{\xi}$ and $\widehat{\boldsymbol{R}}$ to construct the corresponding fingerprint. The covariance matrix $\widehat{\boldsymbol{R}}_{r,t}$ of the r-th channel at the t-th training point can be calculated from the averaged CSI sequence $\boldsymbol{x}_r^u$. While $\boldsymbol{\xi}$ cannot be obtained directly, so we use the eigenspace decomposition method to estimate $\boldsymbol{\xi}$. The estimation process of the projection matrix $\boldsymbol{\xi}_{r,t}$ of the r-th channel at the t-th training point is as follows:

1) Calculate the covariance matrix $\widehat{\boldsymbol{R}}_{r,t}$ by $\hat{\boldsymbol{R}}_{r,t} = \frac{1}{U}\sum_{u=1}^{U} \boldsymbol{x}_r^u \boldsymbol{x}_r^{uH}$
2) Perform an eigenvalue decomposition of $\widehat{\boldsymbol{R}}_{r,t}$
3) Estimate the signal subspace dimension $\widehat{d}$
4) Extract the first $\widehat{d}$ feature vectors of $\widehat{\boldsymbol{R}}_{r,t}$ and obtain $\boldsymbol{V}_{\widehat{d}} = \left\{v_1, \ldots, v_{\widehat{d}}\right\}$
5) Estimate the projection matrix by $\widehat{\boldsymbol{\xi}}_{r,t} = \boldsymbol{V}_{\widehat{d}} \left(\boldsymbol{V}_{\widehat{d}}^H \boldsymbol{V}_{\widehat{d}}\right)^{-1} \boldsymbol{V}_{\widehat{d}}^H$

The projection subspace $\left\{\hat{\boldsymbol{R}}_{r,t}, \boldsymbol{\varphi}_{r,t}\right\}$ from different antennas are composed to form the whole fingerprint $\left\{\hat{\boldsymbol{R}}_t, \boldsymbol{\varphi}_t\right\}$ of the t-th reference point, and then the entire offline fingerprint database is built.

2) ELM NEURAL NETWORK IMPLEMENTATION

Considering that the functional relationship between $\left\{\hat{\boldsymbol{R}}_t, \boldsymbol{\varphi}_t\right\}$ and the actual position coordinates are unknown, the neural network is applied for learning and predicting the location coordinates. During the training phase, using fingerprint information collected in a certain area, the neural network can learn the nonlinear mapping relationship between fingerprint and position coordinates in that area. In positioning phase, signals are received in the same area and fingerprint information is extracted, subsequently this fingerprint information is processed through the neural network to yield the position coordinates. An ensemble of a single-layer neural network called ELM is appled in this paper. This network has the following two advantages

- The network has only one hidden layer. The weights and biases from the input layer to the hidden layer are randomly set in advance, which greatly improves the training speed.
- The connecting weights between the hidden layer and the output layer do not need to be adjusted iteratively. They are determined once by solving the system equations.

The ELM neural network [42] is indeed significantly different from the traditional method. In optimization theory, the introduction of randomness usually helps to enhance the generalization ability of the algorithm. The method of randomizing the hidden layer of the ELM neural network can greatly increase the computing speed and can meet the requirements of high real-time performance of positioning services. This is why the ELM neural network is chosen to learn and predict the position in this paper. As shown in Fig 5, the network includes an input layer, a hidden layer, and an output layer.

The input layer has N neurons, representing the data dimension of an input sample. The hidden layer has S

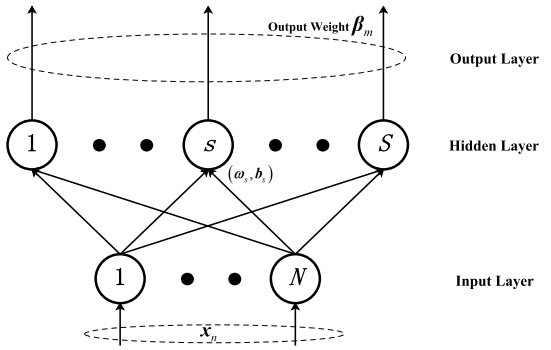

FIGURE 5. ELM network structure.

neurons. The output layer has M neurons which denotes M category labels.

Suppose the connection weight matrix $\boldsymbol{\omega}$ between the input layer and the hidden layer is

$$\boldsymbol{\omega} = \begin{bmatrix} \omega_{11} & \omega_{12} & \dots & \omega_{1N} \\ \omega_{21} & \omega_{22} & \dots & \omega_{2N} \\ \dots & \dots & \dots & \dots \\ \omega_{S1} & \omega_{S2} & \dots & \omega_{SN} \end{bmatrix}_{S\times N}, \tag{42}$$

where ω_{sn} denotes the connection weight between the n-th neuron of the input layer and the s-th neuron of the hidden layer. The connection weight matrix $\boldsymbol{\beta}$ between the output layer and the hidden layer can be expressed as

$$\boldsymbol{\beta} = \begin{bmatrix} \beta_{11} & \beta_{12} & \dots & \beta_{1M} \\ \beta_{21} & \beta_{22} & \dots & \beta_{2M} \\ \dots & \dots & \dots & \dots \\ \beta_{S1} & \beta_{S2} & \dots & \beta_{SM} \end{bmatrix}_{S\times M}, \tag{43}$$

where β_{sm} denotes the connection weight between the m-th neuron of the output layer and the s-th neuron of the hidden layer. The thresholds of hidden layer neurons can be expressed as

$$\boldsymbol{b} = \begin{bmatrix} b_1 \\ b_2 \\ \vdots \\ b_S \end{bmatrix}_{S\times 1}. \tag{44}$$

Considering there are a total of Q fingerprints and the input data matrix $\boldsymbol{X}$ can be expressed as

$$\boldsymbol{X} = \begin{bmatrix} x_{11} & x_{12} & \dots & x_{1Q} \\ x_{21} & x_{22} & \dots & x_{2Q} \\ \dots & \dots & \dots & \dots \\ x_{N1} & x_{N2} & \dots & x_{NQ} \end{bmatrix}_{N\times Q}. \tag{45}$$

Suppose the activation function is $g(\cdot)$and the network's output is equal to the actual sample label $\boldsymbol{O}_q$. Then the final output label set of the network can be written as

$$\boldsymbol{O}_q = \begin{bmatrix} o_{1q} \\ o_{2q} \\ \vdots \\ o_{Mq} \end{bmatrix}_{M\times 1} \quad (q = 1, 2, \dots, Q)$$

$$= \begin{bmatrix} \sum_{s=1}^{S} \beta_{s1} g\left(\boldsymbol{\omega}_s \boldsymbol{x}_q + b_s\right) \\ \sum_{s=1}^{S} \beta_{s2} g\left(\boldsymbol{\omega}_s \boldsymbol{x}_q + b_s\right) \\ \vdots \\ \sum_{s=1}^{S} \beta_{sM} g\left(\boldsymbol{\omega}_s \boldsymbol{x}_q + b_s\right) \end{bmatrix}_{M\times 1}, \tag{46}$$

where $\boldsymbol{\omega}_s = [\omega_{s1}, \omega_{s2}, \dots, \omega_{sN}]$, $\boldsymbol{x}_q = \left[x_{1q}, x_{2q}, \dots, x_{Nq}\right]^T$.

Equation(46) can be written as the following matrix form

$$\boldsymbol{G}\boldsymbol{\beta} = \boldsymbol{O}^T, \tag{47}$$

where

$$\boldsymbol{G}\left(\boldsymbol{\omega}_1, \boldsymbol{\omega}_2, \dots, \boldsymbol{\omega}_S, \boldsymbol{b}_1, \boldsymbol{b}_2, \dots, \boldsymbol{b}_l, \boldsymbol{x}_1, \boldsymbol{x}_2, \dots \boldsymbol{x}_Q\right)$$
$$= \begin{bmatrix} g\left(\boldsymbol{\omega}_1 \boldsymbol{x}_1 + \boldsymbol{b}_1\right) & g\left(\boldsymbol{\omega}_2 \boldsymbol{x}_1 + \boldsymbol{b}_2\right) & \dots & g\left(\boldsymbol{\omega}_S \boldsymbol{x}_1 + \boldsymbol{b}_S\right) \\ g\left(\boldsymbol{\omega}_1 \boldsymbol{x}_2 + \boldsymbol{b}_1\right) & g\left(\boldsymbol{\omega}_2 \boldsymbol{x}_2 + \boldsymbol{b}_2\right) & \dots & g\left(\boldsymbol{\omega}_S \boldsymbol{x}_2 + \boldsymbol{b}_S\right) \\ \dots & \dots & \dots & \dots \\ g\left(\boldsymbol{\omega}_1 \boldsymbol{x}_Q + \boldsymbol{b}_1\right) & g\left(\boldsymbol{\omega}_2 \boldsymbol{x}_Q + b_2\right) & \dots & g\left(\boldsymbol{\omega}_S \boldsymbol{x}_Q + \boldsymbol{b}_S\right) \end{bmatrix}_{Q\times S} \tag{48}$$

For any Q different fingerprint set $\left(\boldsymbol{x}_q, \boldsymbol{O}_q\right)$, $\boldsymbol{x}_q = \left[x_{1q}, x_{2q}, \dots, x_{Nq}\right]^T \in R^N$, $\boldsymbol{O}_q = \left[x_{1q}, x_{2q}, \dots, x_{Mq}\right]^T \in R^M$, assuming that the number of input samples is equal to the number of neurons in the hidden layer, and the activation function is infinitely differentiable in any interval, then for any given $\boldsymbol{\omega}_q$ and $\boldsymbol{b}_q$, the output matrix $\boldsymbol{G}$ of the single-layer network is invertible and satisfies $\|\boldsymbol{G}\boldsymbol{\beta} - \boldsymbol{O}^T\| = 0$. Therefore, when the number of input samples is equal to the number of neurons in the hidden layer, even if $\boldsymbol{\omega}$ and $\boldsymbol{b}$ are randomly selected, the neural network can also approach the training samples with zero error.

In practice, the number of training samples is relatively large. In order to simplify the computational complexity, the number of hidden layer neurons selected is less than the number of training samples. For an arbitrarily small error $\epsilon > 0$ and an infinitely differentiable function $g(\cdot)$ in an arbitrary interval, there is always a single hidden layer feedforward neural network containing $S(S < Q)$ hidden layer neurons. For any $\boldsymbol{\omega}$ and $\boldsymbol{b}$, $\|\boldsymbol{G}\boldsymbol{\beta} - \boldsymbol{O}^T\| < \epsilon$ always meets.

Based on the above principle, even if the number of training samples is relatively large, the final training error of the network will approach a certain value. Therefore, $\boldsymbol{\omega}$ and $\boldsymbol{b}$ of the network can be randomly set in advance and the connection weight $\boldsymbol{\beta}$ can be determined by the following formula

$$\min_{\boldsymbol{\beta}} \|\boldsymbol{G}\boldsymbol{\beta} - \boldsymbol{O}^T\|, \tag{49}$$

and the solution is $\boldsymbol{\beta} = \boldsymbol{G}^{-1}\boldsymbol{O}^T$.

The basic ELM only considers the empirical error minimization of the training data set, which is prone to overfitting. Next, we perform a two-norm constraint method on the weight matrix to optimize it. Considering the goal of network training is to minimize the norm of training error $\|\boldsymbol{O}^T - \boldsymbol{G}\boldsymbol{\beta}\|^2$ and output weight $\|\boldsymbol{\beta}\|^2$, the training process can be expressed as a constrained optimization problem [43]

$$\min_{\boldsymbol{\beta}} \quad \frac{1}{2}\|\boldsymbol{\beta}\|^2 + \frac{1}{2}C\|\boldsymbol{\zeta}\|^2$$

$$\text{s.t.} \quad \boldsymbol{G} \cdot \boldsymbol{\beta} = \boldsymbol{O}^T - \boldsymbol{\zeta}, \tag{50}$$

where C is the regularization coefficient, $\boldsymbol{\zeta}$ is the output error. For the optimization problem with equality constraints, the Lagrangian multiplier method is usually used. After solving the optimization problem we can get $\boldsymbol{\beta}$ as [43]

$$\boldsymbol{\beta} = \boldsymbol{G}^T \left(\frac{I}{C} + \boldsymbol{G}\boldsymbol{G}^T \right)^{-1} \boldsymbol{O}^T. \tag{51}$$

Here we consider that the estimated coordinate position is equal to the position corresponding to the network's output label. However, a single ELM network has only one hidden layer, which limits its performance. What's more, the randomness nature of ELM makes it unstable. Refer to our previous work [40], several ELM networks with the same number of hidden neurons but different weights and bias are jointly optimized to improve the positioning performance. We average the output results of multiple ELM networks to obtain the final estimated location coordinates.

D. COMPUTATIONAL COMPLEXITY ANALYSIS

The computational complexity of the LOS/NLOS recognition stage is $O(L)$, where L represents the channel measurement length. The proposed improved MUSIC algorithm does not introduce any additional computational complexity, as it maintains a complexity of $O(K^3 + M_0K^2)$. Here, K denotes the number of virtual antennas, and M_0 represents the number of spatial spectral search points.In terms of the fingerprint algorithm, which is based on an ELM network, the primary computational complexity during localization arises from subspace feature extraction, which can be expressed as $O(I^3 + S)$, with S denoting the number of neurons in the network and I denoting the number of symbols in a receiving cycle period. In summary, the complexity of the MUSIC algorithm is slightly higher but the positioning accuracy is also higher, while the fingerprint algorithm has a lower complexity and accuracy in the positioning stage. As HyLoc combines these two algorithms, its overall computational complexity will fall between the two extremes, depending on the probability of LOS conditions. K and I can be selected based on the actual situation, thereby controlling the algorithm complexity within an acceptable range.

IV. EXPERIMENTAL RESULTS

In this section, the proposed HyLoc are compared with several existing schemes by simulation. The experiment setup is firstly introduced. Then we verify the performance of each sub algorithm of the proposed Hyloc algorithm. Finally, we verify the positioning performance of the proposed Hyloc algorithm and compare it with other algorithms.

A. EXPERIMENT SETUP

In order to verify the performance of the HyLoc proposed in this paper, the ZedBoard software radio platform is used to obtain practical CSI information. ZedBoard is a low-cost development board based on the Xilinx Zynq-7000 extended processing platform. The main parameters of ZedBoard are shown in Table 1:

TABLE 1. ZedBoard main parameters.

Hardware	Parameter
Chip Model	Zynq-7000 EPP XC7Z020-CLG484-1
RAM	512 MB DDR3
Flash Memory	256 Mb Quad-SPI
SD Card	4 GB
Download Interface	USB-JTAG
Ethernet Interface	10/100/1000
USB	USB OTG 2.0 and USB-UART
Expansion Port	PS & PL I/O
Video Output	1080p HDMI, 8-bit VGA, 128 x 32 OLED
Video Codec	I2S

TABLE 2. Experimental parameters.

Hardware	Parameter
Number of Transmitting Antennas	2
Number of Receiving Antennas	2
Center Frequency	2GHz
Number of Subcarriers	600
Number of OFDM Symbols	31500
System Bandwidth	10MHz
CSI Matrix	$600 \times 31500 \times 2 \times 2$

The laboratory is used as the test scenario to obtain actual CSI information. In order to simulate a real environment, there are people moving around during the experiment.

Two development boards are used in the experiment to simulate a simple sending and receiving process based on the LTE protocol on a PC. In the data collection phase, the position of the transmitter is fixed and the receiver is placed on a pre-divided grid point. A downlink transmitting program keeps running on the transmitter platform at the frequency of 2GHz. The floor plan of the laboratory is shown in the Fig. 6. We divided the laboratory, with an approximate area of $50m^2$, into a grid of square cells with side length $0.5m$. And we use these 105 grid points as training points. Some of points are LOS and some are NLOS to consider the LOS/NLOS mixed scenario. In addition, we randomly selected 12 non-grid points as test points. At each point, the receiver continuously receives signal packets and extracts CSI, repeating multiple times at the same point to obtain sufficient measurement data. In this experiment the signal bandwidth is 10MHz and the signal reception duration is 0.2s. The final extracted CSI is a $600 \times 31500 \times 2 \times 2$ tensor for each point, representing 600 subcarriers in the frequency domain, 31500 OFDM symbols in the time domain and 2×2 *multi-input multi-output* (MIMO) in the spatial domain. The specific experimental parameters are shown in Table 2.

B. LOS/NLOS IDENTIFICATION PERFORMANCE

We first verified the effectiveness of the proposed LOS/NLOS identification algorithm. Fig.7 shows the identification accuracy of the proposed method at different distances from the transmitter. In our experimental environment, the proposed method achieves a NLOS identification accuracy of 88% for all sampling points. And it can be

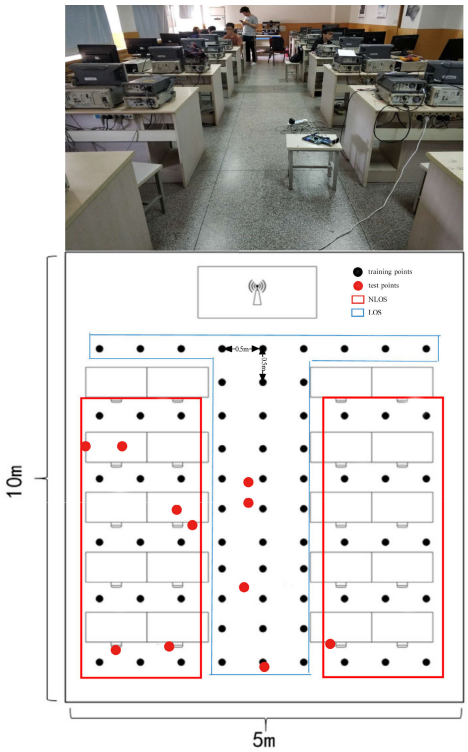

FIGURE 6. The floor plan of the laboratory.

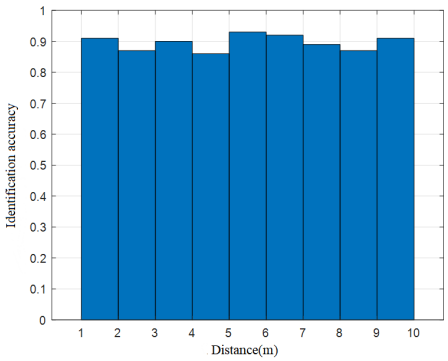

FIGURE 7. LOS/NLOS identification accuracy at different distances from the transmitter.

observed that there is no direct correlation between LOS identification accuracy and propagation distance. This is because the proposed method utilizes statistical features of the signal, which are unrelated to the overall signal strength. This result proves the effectiveness of the proposed method and serves as the foundation for subsequent positioning.

C. IMPROVED MUSIC PERFORMENCE

In this section we conducted a comparison between the improved MUSIC algorithm and the classic MUSIC algorithm. Fig. 8 present the spatial spectrum generated by both algorithms for the same point. It is evident that the classic MUSIC algorithm may overlook the peak, while the improved algorithm, after undergoing smoothing, reveals two new peaks near the $-30°$ arrival angle. This is because one source may generate highly correlated multipath signals

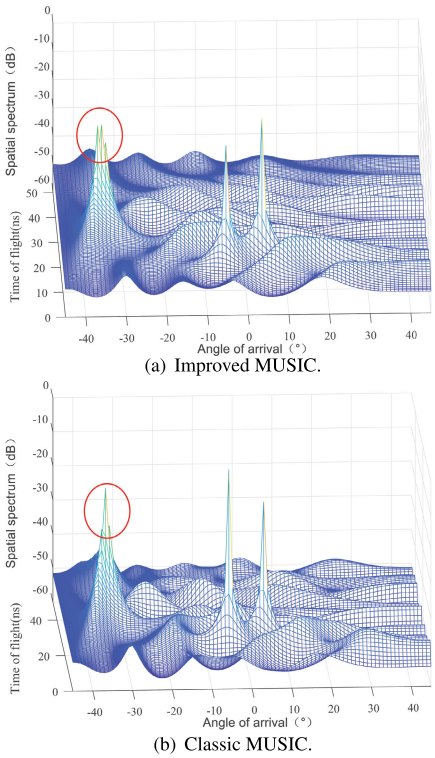

FIGURE 8. The spatial spectrum of diffirence method.

after passing through similar propagation paths, resulting in the classical MUSIC algorithm being unable to distinguish between different paths. Similar phenomena were observed at many points in the experiment, which demonstrates that smoothing processing can effectively eliminate the occurrence of missed or misjudged peaks and enhances the robustness of the algorithm when relevant sources exist.

D. COMPARING THE POSITIONING ACCURACY OF FINGERPRINT AND MUSIC ALGORITHM

We divided the test points into NLOS and LOS sections, and used two methods to locate all test points. Each point was repeated multiple times and the positioning error was counted. Fig. 9 shows the positioning performance of two methods in two different environments. It can be clearly observed that in LOS environments, the MUSIC algorithm achieves higher localization accuracy, while in NLOS environments, the fingerprinting algorithm achieves higher localization accuracy. Therefore, the idea of using MUSIC algorithm in LOS scenario and fingerprint algorithm in NLOS scenario is reasonable in the proposed Hybrid localization algorithm.

E. POSITIONING ACCURACY OF PROPOSED HYLOC

The Hyloc algorithm proposed in this paper leverages LOS/NLOS identification to fully exploit the strengths of both methods, thereby achieving higher positioning accuracy in mixed LOS/NLOS environments. The positioning results of the HyLoc is shown in Fig. 10 and Fig. 12.

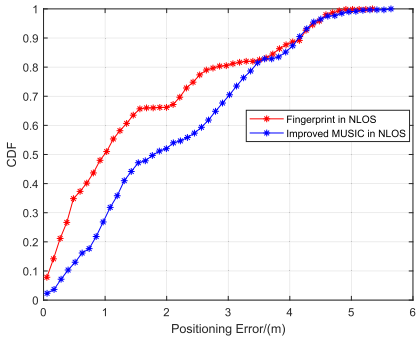

(a) NLOS.

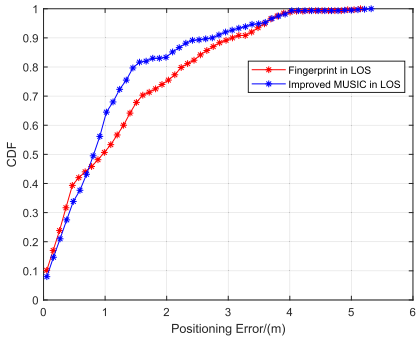

(b) LOS.

FIGURE 9. Positioning error cumulative distribution function (CDF) of diffirence method in different scenarios.

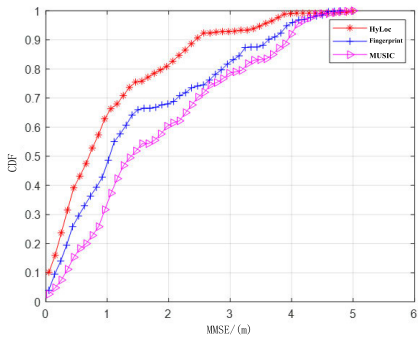

FIGURE 10. Comparison of Hybrid positioning scheme and single positioning method.

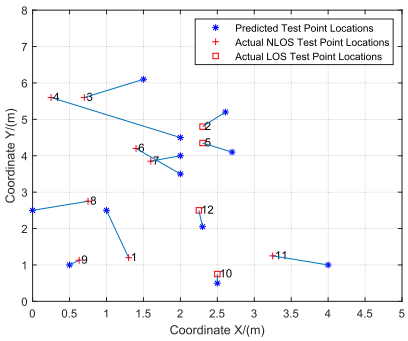

FIGURE 11. The floor plan of positioning effect.

It can be seen from Fig. 10 that when the improved MUSIC algorithm is singly used, it shows poor positioning results. This is because the positioning method based on parameter estimation is highly dependent on the propagation environment, and the existence of NLOS paths greatly increase the

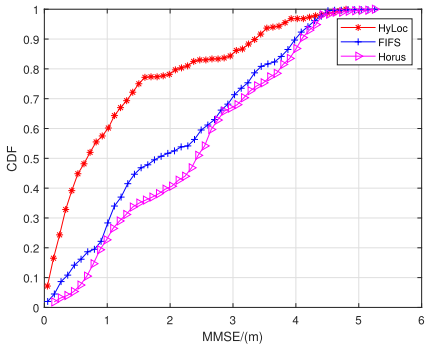

FIGURE 12. Comparison of existing classic methods.

TABLE 3. Comparison of errors in different positioning methods.

Method	MMSE(m)	Median error(m)
HyLoc	1.6140	1.1342
FIFS	2.0862	2.2233
FILA	1.9067	1.9263

estimation error. When the fingerprint positioning algorithm is singly used, the performance is better than that of improved MUSIC algorithm. It also shows that the positioning results of the fingerprint method is less affected by the environment. Finally, through LOS/NLOS identification and integrating the two positioning methods, it can be obviously seen that the performance of the proposed HyLoc is the best, which proves the effectiveness of the hybrid scheme.

Fig. 11 is an intuitive positioning result diagram of the HyLoc. A total of 12 test points are selected. It can be seen that although several points have large errors, most points can achieve good positioning results. Among them, the general positioning results of the points with LOS path is better than that of points with NLOS paths.

We also compare our proposed hybrid positioning scheme with Hours [19] and FIFS [20] systems, which are two classic positioning methods. The obtained *minimum mean square error* (MMSE) distance and median error distance are shown in Table 3, and the obtained *cumulative distribution function* (CDF) curve of MMSE is shown in Fig. 12. It can be seen that the performance of the HyLoc is much better than the other two positioning systems. Using the HyLoc, the position coordinate MMSE of 80% test points is within $2m$. The proposed HyLoc can achieve the best positioning accuracy. In terms of algorithm complexity, as both FIFS and Hour algorithms are fingerprint based positioning algorithms, their positioning phase has a similar complexity to the fingerprint algorithm proposed in this paper and lower then improved MUSIC. However, these two methods do not fully utilize the fingerprint information in the received signal, nor do they utilize the information of the direct path, resulting in lower positioning accuracy.

V. CONCLUSION

Aiming at the problem of unsatisfactory positioning performance in mixed LOS and NLOS environment, this paper proposes a hybrid localization method based on

LOS/NLOS identification which realizes single-site localization. Depending on the different probability distributions of RPS in different propagation environments, four statistical characteristics are firstly calculated and a TJ is designed to identify whether there is a LOS path in the environment. According to the identification results of TJ, the HyLoc adaptively select the optimal positioning method. For the environment with LOS paths, MUSIC algorithm is used to estimate the positioning parameters, and the forward smoothing technology is used to eliminate the influence of coherent signals. For the environment with NLOS path, the MSP and ELM-based fingerprint localization algorithm is propsoed to complete positioning, using a signal subspace method to do dimensionality reduction and signal feature extraction, and an ensemble of ELM network to estimate the positioning results. Finally, the experimental results show that the HyLoc proposed in this paper can realize single-site localization and has better positioning performance than the single method and several existing classic positioning methods.

APPENDIX A
DERIVATION OF EQUATION (38)

From (37), the log likelihood function of the received signal can be expressed as

$$\begin{aligned}&\log p\left(\boldsymbol{x}_r^1,\ldots,\boldsymbol{x}_r^U \mid \boldsymbol{A}_r,\boldsymbol{\Gamma},\sigma^2\right)\\ =&C-IU\log\sigma^2-\sum_{u=1}^{U}\frac{1}{\sigma^2}\left\|\boldsymbol{x}_r^u-\boldsymbol{A}_r\boldsymbol{\gamma}^u\right\|^2,\end{aligned}\tag{52}$$

where C is a constant. After removing the constant term, the maximum likelihood estimation of $\boldsymbol{A}_r$ can be expressed as

$$\begin{aligned}\left[\widehat{\boldsymbol{A}}_r,\widehat{\boldsymbol{\Gamma}},\widehat{\sigma}^2\right]&=\arg\max_{\boldsymbol{A}_r,\boldsymbol{\Gamma},\sigma^2}\log p\left(\boldsymbol{x}_r^1,\ldots,\boldsymbol{x}_r^U \mid \boldsymbol{A}_r,\boldsymbol{\Gamma},\sigma^2\right)\\&=\arg\min_{\boldsymbol{A}_r,\boldsymbol{\Gamma},\sigma^2} IU\log\sigma^2+\frac{1}{\sigma^2}\sum_{u=1}^{U}\left\|\boldsymbol{x}_r^u-\boldsymbol{A}_r\boldsymbol{\gamma}^u\right\|^2.\end{aligned}\tag{53}$$

Taking the partial derivative of $\boldsymbol{\gamma}^u$ and σ^2 and setting them to 0, we obtain the maximum likelihood estimate of $\boldsymbol{\gamma}^u$ and σ^2 as

$$\widehat{\boldsymbol{\gamma}}^u=\left(\boldsymbol{A}_r^H\boldsymbol{A}\right)^{-1}\boldsymbol{A}^H\boldsymbol{x}_r^u.\tag{54}$$

$$\widehat{\sigma}^2=\frac{\sum_{u=1}^{U}\left\|\boldsymbol{x}_r^u-\boldsymbol{A}_r\boldsymbol{\gamma}^u\right\|^2}{IU}.\tag{55}$$

Subsequently, substituting (54) and (55) into (53) we can obtain

$$\begin{aligned}\widehat{\boldsymbol{A}}_r&=\arg\min_{\boldsymbol{A}_r} IU\log\frac{\sum_{u=1}^{U}\left\|\boldsymbol{x}_r^u-\boldsymbol{\xi}\boldsymbol{x}_r^u\right\|^2}{IU}+IU\\&=\arg\min_{\boldsymbol{A}_r}\sum_{u=1}^{U}\|\boldsymbol{x}_r^u-\boldsymbol{\xi}\boldsymbol{x}_r^u\|^2,\end{aligned}\tag{56}$$

which is equation (38).

REFERENCES

[1] Y. Li, Y. Zhuang, X. Hu, Z. Gao, J. Hu, L. Chen, Z. He, L. Pei, K. Chen, M. Wang, X. Niu, R. Chen, J. Thompson, F. M. Ghannouchi, and N. El-Sheimy, "Toward location-enabled IoT (LE-IoT): IoT positioning techniques, error sources, and error mitigation," *IEEE Internet Things J.*, vol. 8, no. 6, pp. 4035–4062, Mar. 2021.

[2] A. Li, J. Fu, H. Shen, and S. Sun, "A cluster-principal-component-analysis-based indoor positioning algorithm," *IEEE Internet Things J.*, vol. 8, no. 1, pp. 187–196, Jan. 2021.

[3] W. Zhang, K. Yu, W. Wang, and X. Li, "A self-adaptive AP selection algorithm based on multiobjective optimization for indoor WiFi positioning," *IEEE Internet Things J.*, vol. 8, no. 3, pp. 1406–1416, Feb. 2021.

[4] S. Sadowski, P. Spachos, and K. N. Plataniotis, "Memoryless techniques and wireless technologies for indoor localization with the Internet of Things," *IEEE Internet Things J.*, vol. 7, no. 11, pp. 10996–11005, Nov. 2020.

[5] J. Hu, D. Liu, Z. Yan, and H. Liu, "Experimental analysis on weight K-nearest neighbor indoor fingerprint positioning," *IEEE Internet Things J.*, vol. 6, no. 1, pp. 891–897, Feb. 2019.

[6] H. Li, Z. Qian, C. Tian, and X. Wang, "TILoc: Improving the robustness and accuracy for fingerprint-based indoor localization," *IEEE Internet Things J.*, vol. 7, no. 4, pp. 3053–3066, Apr. 2020.

[7] E. Y. Menta, N. Malm, R. Jäntti, K. Ruttik, M. Costa, and K. Leppänen, "On the performance of AoA–based localization in 5G ultra–dense networks," *IEEE Access*, vol. 7, pp. 33870–33880, 2019.

[8] J. Chadha and A. Jain, "Anatomization on range-free localization algorithms in wireless sensor networks," in *Proc. 2nd Int. Conf. Power Energy, Environ. Intell. Control (PEEIC)*, Oct. 2019, pp. 489–492.

[9] C. Gao, G. Wang, and S. G. Razul, "Comparisons of the super-resolution TOA/TDOA estimation algorithms," in *Proc. Prog. Electromagn. Res. Symp. Fall (PIERS-FALL)*, Nov. 2017, pp. 2752–2758.

[10] H. Xiong, M. Peng, S. Gong, and Z. Du, "A novel hybrid RSS and TOA positioning algorithm for multi-objective cooperative wireless sensor networks," *IEEE Sensors J.*, vol. 18, no. 22, pp. 9343–9351, Nov. 2018.

[11] X. Li and K. Pahlavan, "Super-resolution TOA estimation with diversity for indoor geolocation," *IEEE Trans. Wireless Commun.*, vol. 3, no. 1, pp. 224–234, Jan. 2004.

[12] V. U. Prabhu and D. Jalihal, "An improved ESPRIT based time-of-arrival estimation algorithm for vehicular OFDM systems," in *Proc. IEEE 69th Veh. Technol. Conf.(VTC Spring)*, Apr. 2009, pp. 1–4.

[13] K. Witrisal, P. Meissner, E. Leitinger, Y. Shen, C. Gustafson, F. Tufvesson, K. Haneda, D. Dardari, A. F. Molisch, A. Conti, and M. Z. Win, "High-accuracy localization for assisted living: 5G systems will turn multipath channels from foe to friend," *IEEE Signal Process. Mag.*, vol. 33, no. 2, pp. 59–70, Mar. 2016.

[14] J. Fan, S. Chen, X. Luo, Y. Zhang, and G. Y. Li, "A machine learning approach for hierarchical localization based on multipath MIMO fingerprints," *IEEE Commun. Lett.*, vol. 23, no. 10, pp. 1765–1768, Oct. 2019.

[15] N. Etemadyrad and J. K. Nelson, "A sequential detection approach to indoor positioning using RSS-based fingerprinting," in *Proc. IEEE Global Conf. Signal Inf. Process. (GlobalSIP)*, Dec. 2016, pp. 1127–1131.

[16] X. Li and J. Zhu, "Improved indoor positioning method based on CSI," in *Proc. Int. Conf. Intell. Transp., Big Data Smart City (ICITBS)*, Jan. 2019, pp. 274–277.

[17] Y. Zhang, D. Li, and Y. Wang, "An indoor passive positioning method using CSI fingerprint based on AdaBoost," *IEEE Sensors J.*, vol. 19, no. 14, pp. 5792–5800, Jul. 2019.

[18] P. Bahl and V. N. Padmanabhan, "RADAR: An in-building RF-based user location and tracking system," in *Proc. IEEE Conf. Comput. Commun. (INFOCOM), 19th Annu. Joint Conf. IEEE Comput. Commun. Societies*, Mar. 2000, pp. 775–784.

[19] M. Youssef and A. Agrawala, "The Horus WLAN location determination system," in *Proc. 3rd Int. Conf. Mobile Syst., Appl., Services*, Jun. 2005, pp. 205–218.

[20] J. Xiao, K. Wu, Y. Yi, and L. M. Ni, "FIFS: Fine-grained indoor fingerprinting system," in *Proc. 21st Int. Conf. Comput. Commun. Netw. (ICCCN)*, Jul. 2012, pp. 1–7.

[21] C. Xu, B. Firner, Y. Zhang, and R. E. Howard, "The case for efficient and robust RF-based device-free localization," *IEEE Trans. Mobile Comput.*, vol. 15, no. 9, pp. 2362–2375, Sep. 2016.

[22] P. Davidson and R. Piché, "A survey of selected indoor positioning methods for smartphones," *IEEE Commun. Surveys Tuts.*, vol. 19, no. 2, pp. 1347–1370, 2nd Quart., 2017.
[23] H. Chen, Y. Zhang, W. Li, X. Tao, and P. Zhang, "ConFi: Convolutional neural networks based indoor Wi-Fi localization using channel state information," *IEEE Access*, vol. 5, pp. 18066–18074, 2017.
[24] Z. Abu-Shaban, X. Zhou, and T. D. Abhayapala, "A novel TOA-based mobile localization technique under mixed LOS/NLOS conditions for cellular networks," *IEEE Trans. Veh. Technol.*, vol. 65, no. 11, pp. 8841–8853, Nov. 2016.
[25] C.-H. Park and J.-H. Chang, "Robust LMedS-based WLS and Tukey-based EKF algorithms under LOS/NLOS mixture conditions," *IEEE Access*, vol. 7, pp. 148198–148207, 2019.
[26] Y. Li, S. Ma, G. Yang, and K.-K. Wong, "Robust localization for mixed LOS/NLOS environments with anchor uncertainties," *IEEE Trans. Commun.*, vol. 68, no. 7, pp. 4507–4521, Jul. 2020.
[27] S. Zhang, S. Gao, G. Wang, and Y. Li, "Robust NLOS error mitigation method for TOA-based localization via second-order cone relaxation," *IEEE Commun. Lett.*, vol. 19, no. 12, pp. 2210–2213, Dec. 2015.
[28] G. Wang, H. Chen, Y. Li, and N. Ansari, "NLOS error mitigation for TOA-based localization via convex relaxation," *IEEE Trans. Wireless Commun.*, vol. 13, no. 8, pp. 4119–4131, Aug. 2014.
[29] R. M. Vaghefi and R. M. Buehrer, "Cooperative localization in NLOS environments using semidefinite programming," *IEEE Commun. Lett.*, vol. 19, no. 8, pp. 1382–1385, Aug. 2015.
[30] T. Qiao and H. Liu, "Improved least median of squares localization for non-line-of-sight mitigation," *IEEE Commun. Lett.*, vol. 18, no. 8, pp. 1451–1454, Aug. 2014.
[31] F. Yin, C. Fritsche, F. Gustafsson, and A. M. Zoubir, "EM- and JMAP-ML based joint estimation algorithms for robust wireless geolocation in mixed LOS/NLOS environments," *IEEE Trans. Signal Process.*, vol. 62, no. 1, pp. 168–182, Jan. 2014.
[32] I. Guvenc, C.-C. Chong, and F. Watanabe, "NLOS identification and mitigation for UWB localization systems," in *Proc. IEEE Wireless Commun. Netw. Conf.*, Mar. 2007, pp. 1571–1576.
[33] D. Jin, F. Yin, M. Fauß, M. Muma, and A. M. Zoubir, "Exploiting sparsity for robust sensor network localization in mixed LOS/NLOS environments," in *Proc. IEEE Int. Conf. Acoust., Speech Signal Process. (ICASSP)*, May 2020, p. 5915.
[34] S. Maranò, W. M. Gifford, H. Wymeersch, and M. Z. Win, "NLOS identification and mitigation for localization based on UWB experimental data," *IEEE J. Sel. Areas Commun.*, vol. 28, no. 7, pp. 1026–1035, Sep. 2010.
[35] B. Hu, H. Tian, and S. Fan, "Millimeter wave LOS/NLOS identification and localization via mean-shift clustering," in *Proc. IEEE 30th Annu. Int. Symp. Pers., Indoor Mobile Radio Commun. (PIMRC)*, Sep. 2019, pp. 1–7.
[36] G. Qing, K. Wei, and T. Wanchun, "Wireless positioning method based on dynamic objective function under mixed LOS/NLOS conditions," in *Proc. Ubiquitous Positioning, Indoor Navigat. Location-Based Services (UPINLBS)*, Mar. 2018, pp. 1–4.
[37] K. Yu, K. Wen, Y. Li, S. Zhang, and K. Zhang, "A novel NLOS mitigation algorithm for UWB localization in harsh indoor environments," *IEEE Trans. Veh. Technol.*, vol. 68, no. 1, pp. 686–699, Jan. 2019.
[38] X. Wang, L. Gao, and S. Mao, "CSI phase fingerprinting for indoor localization with a deep learning approach," *IEEE Internet Things J.*, vol. 3, no. 6, pp. 1113–1123, Dec. 2016.
[39] T.-J. Shan, M. Wax, and T. Kailath, "On spatial smoothing for direction-of-arrival estimation of coherent signals," *IEEE Trans. Acoust., Speech, Signal Process.*, vol. ASSP-33, no. 4, pp. 806–811, Apr. 1985.
[40] J. Fan, H. Sun, Y. Su, and J. Huang, "MuSpel-Fi: Multipath subspace projection and ELM-based fingerprint localization," *IEEE Signal Process. Lett.*, vol. 29, pp. 329–333, 2022.
[41] E. Kupershtein, M. Wax, and I. Cohen, "Single-site emitter localization via multipath fingerprinting," *IEEE Trans. Signal Process.*, vol. 61, no. 1, pp. 10–21, Jan. 2013.
[42] G.-B. Huang, Q.-Y. Zhu, and C.-K. Siew, "Extreme learning machine: Theory and applications," *Neurocomputing*, vol. 70, nos. 1–3, pp. 489–501, Dec. 2006.
[43] G.-B. Huang, H. Zhou, X. Ding, and R. Zhang, "Extreme learning machine for regression and multiclass classification," *IEEE Trans. Syst. Man, Cybern. B, Cybern.*, vol. 42, no. 2, pp. 513–529, Apr. 2012.

JINBO ZHANG received the Ph.D. degree in signal and information processing from the Beijing University of Posts and Telecommunications, Beijing, China, in 2014. He is currently a Senior Engineer with the Science and Technology on Communication Networks Laboratory, The 54th Research Institute of CETC, Shijiazhuang, China. His general research interests include signal processing and wireless communications, with an emphasis on MIMO communication technology, practical issues in 5G and 6G systems, and microwave/millimeter wave/terahertz communication systems. In these areas, he has published more than 20 journals and conference papers, and has filed more than ten patents in recent years.

HAO SUN received the B.S. degree from Xidian University, Xi'an, China, in 2020. He is currently pursuing the M.S. degree with Xi'an Jiaotong University, Xi'an. His general research interests include indoor high-precision positioning technology and 5G key technology.

YUJIE FENG received the B.S. degree from Xi'an Jiaotong University, Xi'an, China, in 2021, where he is currently pursuing the M.S. degree. His general research interests include channel parameter estimation and high-precision positioning technology.

JIANCUN FAN (Senior Member, IEEE) received the B.S. and Ph.D. degrees in electrical engineering from Xi'an Jiaotong University, Xi'an, Shaanxi, China, in 2004 and 2012, respectively. From August 2009 to August 2011, he was a Visiting Scholar with the School of Electrical and Computer Engineering, Georgia Institute of Technology, Atlanta, GA, USA. From September 2017 to December 2017, he was a Visiting Scholar with Technische Universitat Dresden (TUD), Germany. He is currently a Professor and the Associate Dean of the School of Information and Communications Engineering, Xi'an Jiaotong University. His general research interests include signal processing and wireless communications, with emphasis on MIMO communication systems, practical issues in 5G and 6G systems, navigation and localization, and machine learning application for wireless communication. In these areas, he has published over 100 journals and conference papers. He was a recipient of the Best Paper Award at the 20th International Symposium on Wireless Personal Multimedia Communications, in 2017.